

A geometric condition for robot-swarm cohesion and cluster-flock transition

Mathias Casiulis,^{1,2} Eden Arbel,³ Yoav Lahini,³ Stefano Martiniani,^{1,2,4} Naomi Oppenheimer,³ and Matan Yah Ben Zion^{5,*}

¹Center for Soft Matter Research, Department of Physics, New York University, New York 10003, USA

²Simons Center for Computational Physical Chemistry, Department of Chemistry, New York University, New York 10003, USA

³School of Physics and Astronomy, and the Center for Physics and

Chemistry of Living Systems, Tel Aviv University, Tel Aviv 6997801, Israel

⁴Courant Institute of Mathematical Sciences, New York University, New York 10003, USA

⁵Department of Artificial Intelligence, Donders Center for Cognition, Radboud University, Nijmegen, Netherlands

We present a geometric design rule for size-controlled clustering of self-propelled particles. Active particles that tend to rotate under an external force have an intrinsic signed-parameter with units of curvature, which we term *curvity*, derivable from first principles. Robot experiments and numerical simulations show that the properties of the individual robot alone — radius and curvity — control pair-cohesion in a binary system as well as the stability of flocking and clustering in a swarm. Our results have applications in meta-materials and embodied decentralized control.

Active matter offers a wealth of behaviors unfathomable at equilibrium: the broken time-reversal-symmetry and lack of Galilean invariance [1–3] unlock new dynamical [4–6], structural [7–14], and functional [3, 15–17] states, that expand the notion of materials to describe both living systems and robotic swarms [18–26]. In equilibrium, the direct link between pair interactions and the emergent structures is established by statistical mechanics [27–29], with applications for multi-scale design. Far from equilibrium however this luxury is largely absent. There are only a handful of cases [30–32] that directly link emergent behavior to the details of the pairwise interaction, hindering the bottom-up design of functional active matter.

In systems of self-propelled particles, the emergence of collective behaviors like flocking or Motility-Induced Phase Separation (MIPS) is now well established [33, 34]. Theoretical predictions rely on the interaction between a particle and an averaged property of its neighbors – a mean-field-like approximation often called quorum sensing [35]. For example, flocking can emerge when a particle aligns with the averaged heading of its neighbors (Vicsek model) [4]; MIPS is observed when a particle slows down with increasing local particle concentration [35, 36]; and a similar crowding is observed when a particle’s heading turns towards locally higher particle concentrations [37], yet it is not obvious *a priori* how the coarse-grained field emerges from the microscopic properties of the individual. This leads to the unsatisfactory situation where prediction, let alone design, of the collective behavior of a large ensemble, requires knowledge of the response of an individual to a smaller ensemble, and does not stem directly from the single particle characteristics.

Microscopic models of self-propelled particles typically describe the direct response of their velocity, \vec{v} , to external forces, \vec{F} , through an effective mobility, μ [38–40]. It was identified empirically that forces also generically couple to the particle’s orientation, \hat{e} , effectively imposing a torque that rotates its heading [41]. A microscopic

link between the particle’s mobility and the associated torque was recently derived from Newtonian mechanics for hopping self-propelled particles [42]. It was shown that it affects the dynamics through a single activity-induced quantity with units of curvature, *curvity*. Crucially, curvity is signed, much like an electric charge. When positive (\hat{e} aligns onto \vec{F}), it leads to orbiting dynamics in a confining potential of an individual [43], and to flocking through collision induced alignment in ensembles [44–46]. When negative (\hat{e} anti-aligns with \vec{F}), it couples to the curvature of passive objects, which can induce cooperative transport of a movable payload through spontaneous symmetry breaking [42].

In this Letter, we show experimentally, numerically, and analytically, that the *curvity* also couples to the curvature of the self-propelled particles themselves. Pairs of particles of radii b , and curvity κ , will display effective attraction when the geometric criterion

$$\kappa + 1/b < 0 \quad (1)$$

is met, which is the main result of our work. Equation 1 conditions the attraction of an active particle to *another* active particle. It establishes pair-cohesion, and extends previous result on the adhesion of a single active particle to a static potential [42]. As demonstrated below, it sets the cornerstone for the many-body behavior. Inequality 1 is geometric in the sense that it compares two intrinsic length scales of the active particle, its curvity, κ , and its curvature, $1/b$ (inverse radius), and depends neither on kinematics (speeds and rates) nor mechanics (forces). We find this criterion holds in experiments using custom-built vibration-driven robots, as well as in Langevin simulations of self-propelled particles, where we varied the particles diameters and curvities. We also present an extension of this criterion to finite densities, that predicts a clustering transition into crystallites of controlled size, paving the way for controlling the large scale behavior of self-propelled particles such as robotic swarms using only

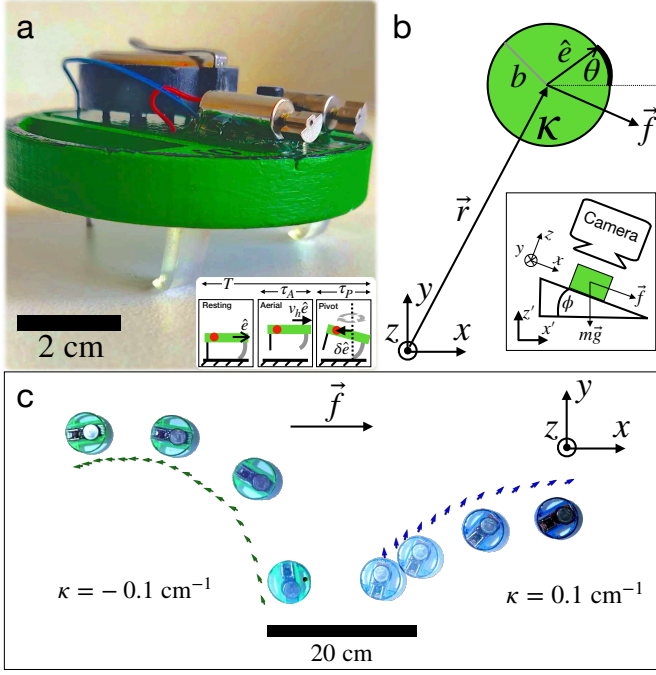


FIG. 1. Measuring the curvity, κ , of a self-propelled particle. (a) A vibration-driven robot (two vibration motors), two soft front legs, and a stiff back leg. Inset illustrates the displaced (δ) center of mass (red dot) from the rotation axis (dashed line) along the heading (\hat{e}) in the aerial and pivot phases of motion resulting in Eqs. 2, 3. (b) The curvity, κ , is measured using an inclined plane to apply a constant force (inset), monitoring the particle's position (\vec{r}) and heading (\hat{e}). (c) Heading rotation along (blue $\kappa > 0$) or against (green $\kappa < 0$) an external constant force (\vec{f}).

local parameters.

We start by analytically investigating the deterministic pair dynamics, showing that the condition in Eq. 1 offers a stable fixed point for pairwise attraction. We then test this criterion experimentally by measuring the *kissing time* (τ_k) — the duration over which two vibration-driven robots osculate. Finally, we test this condition numerically by simulating the many-body dynamics over a range of densities, finding that the condition in Eq. 1 naturally extends to finite concentrations and noises, and quantitatively predicts the size of self-limiting clusters.

Equations of motion. Empirically, the time evolution of the velocity, \vec{v} , and heading $\hat{e} \equiv (\cos \theta, \sin \theta)$, of a self-propelled particle subjected to an external force, \vec{f} , is often captured [41, 47] by the effective equations of motion

$$\frac{d}{dt} \vec{r}(t) \equiv \vec{v}(t) = v_0 \hat{e}(t) + \mu \vec{f}(t), \quad (2)$$

$$\frac{d}{dt} \hat{e}(t) = \kappa \hat{e}(t) \times (\vec{v}(t) \times \hat{e}(t)), \quad (3)$$

where v_0 is the nominal speed, μ the mobility, and κ the curvity of the particle. The curvity, κ , is the first key parameter in our geometric construction. When an external force is perpendicular to the orientation of the

self-propelled particle, the curvity determines how much the trajectory curves to align parallel ($\kappa > 0$) or anti-parallel ($\kappa < 0$) to the force. Curvity is thus analogous to an electric charge: much like a charge q moving along a cyclotron orbit with Larmor radius $R_L \propto 1/q$ when placed in an out-of-plane magnetic field B [48], a self-propelled particle with curvity κ orbits with $R \propto 1/\kappa$ when subjected to a force field perpendicular to its orientation [49].

Equations 2 and 3 were recently derived from the Newtonian dynamics of vibration-driven robots [42], offering their microscopic origin, and a handle for swarm design. In particular the curvity is $\kappa \equiv \delta (\tau_P / \tau_A)^2 m / I$, where τ_A and τ_P are the aloft and pivot times; m and I are the mass and moment of inertia; and δ is the signed displacement of the center of mass from the pivot axis along the heading, $\vec{\delta} \equiv \delta \hat{e}$ (see Fig. 1 and SM [50]). Beyond this example, force-alignment can be pivotal in a large class of “dry” active matter, from shaken granules to bacterial colonies [17, 33] — except for the singular case where the center of mass is directly aligned with the center of stress, one should expect a finite (and signed) curvity.

The second key parameter in the geometric construction is simply the radius of each particle, b . When the steric repulsion between circular particles 1 and 2 is described as a radially symmetric force field, $\vec{F}_{21} \equiv v_0 / \mu \Gamma(r_{21}) \hat{r}$, their mutual dynamics follow

$$\vec{v}_2 = v_0 \hat{e}_2 + \mu \vec{F}_{21} \quad (4)$$

$$\frac{d}{dt} \hat{e}_2 = \kappa \hat{e}_2 \times (\vec{v}_2 \times \hat{e}_2), \quad (5)$$

and $2 \rightarrow 1$ for particle 1 (see Fig. 2a inset). The point where steric repulsion balances self-propulsion, $\Gamma(r_{21} = 2b) \equiv 1$, defines the particles' radii. When the repulsion is spatially decaying ($\Gamma' < 0$) the force profile Γ can be left implicit, and apply for common steric interactions (soft-core, screened Coulomb, WCA etc. [27, 51]), making the following argument general. The 6 degrees of freedom in Eqs. 4, 5 reduce to only 3 relative degrees of freedom in center-of-mass coordinates: the distance between the centers, $|\vec{r}_{21}| = r$, and the relative angle of the headings α, β

$$\dot{r} = v_0 [\cos \alpha + \cos \beta + 2\Gamma(r)] \quad (6)$$

$$\dot{\alpha} = -v_0 \left[\left(\kappa \Gamma(r) + \frac{1}{r} \right) \sin \alpha + \frac{1}{r} \sin \beta \right] \quad (7)$$

$$\dot{\beta} = -v_0 \left[\left(\kappa \Gamma(r) + \frac{1}{r} \right) \sin \beta + \frac{1}{r} \sin \alpha \right], \quad (8)$$

see Fig. 2a inset and SM [50]. When the condition in Eq. 1 is met, the dynamical system in Eqs. 6-8 undergoes a sub-critical pitchfork bifurcation [52], giving rise to a basin of attraction with a linearly stable fixed point when two particles mutually push heads on ($\alpha = \beta = \pi, r = 2b$, see SM [50]). Figures 2a,b show α - r phase-portraits of κb

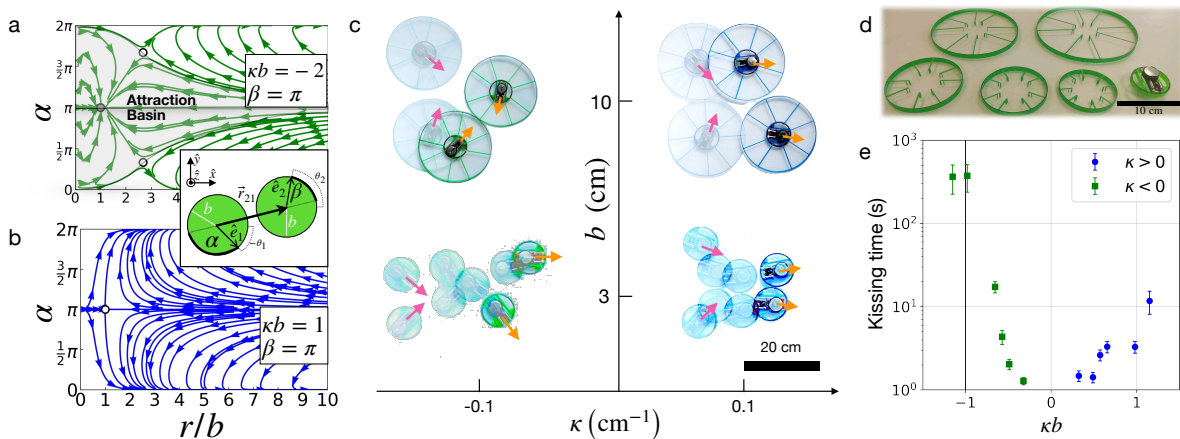


FIG. 2. A geometric criterion for effective pairwise attraction of two self-propelled particles. (a) and (b) show α - r phase portrait of Eqs. 6, 7 at a constant $\beta = \pi$. An attraction basin is found when the geometrical criterion is satisfied (Eq. 1). Inset shows the dynamic variables of two interacting self-propelled particles. (c) The initial (pink) and final (orange) states of pair-collision in vibration driven-robots show effective binding by fronting ($\alpha = \beta \rightarrow \pi$, $r \rightarrow 2b$) when Eq. 1 is satisfied (top left), otherwise the robots scatter. (d) 3D printed skirts of different sizes to change a robot's radius, b . (e) Experimentally measured kissing time (τ_k) shows over 2 orders of magnitude increase when $\kappa b < -1$, inline with the geometric criterion of attraction (Eq. 1).

combinations above and below the bifurcation (at fixed $\beta = \pi$) illustrating the formation of a basin of attraction.

Remarkably, we just proved that a simple, purely geometric criterion, that does not involve any force or time scale, predicts the onset of pair cohesion, regardless of the explicit profile structure of the steric repulsion.

Pair cohesion in vibrational robots. The condition in Eq. 1 is supported experimentally by tuning κ and b in vibration-driven robots, and measuring the average pair kissing time, τ_k . Robots were built by gluing two counter-rotating vibration motors (DC Mini Vibration Motor 14000 RPM), to a PCB and connecting to a battery (LIR2477) through a switch. The electronics circuit is then glued to a 3D printed circular chassis of a typical radius of $b_0 \approx 3$ cm (PLA, Bambu Lab), with a pair of soft legs (Elastic50A Resin, Formlabs), and a stiff leg (stainless steel pin, see Fig. 1a and SM [50]). The individual robots' nominal speeds ($v_0 \approx 3$ cm/s $\approx b_0/s$) was measured by imaging (Sony Alpha R), and tracking (using standard [53, 54] and homemade algorithms) the position (x, y) and orientation (θ) of a robot running on a plate (Perspex), and computing the short time mean square displacement where trajectories are ballistic ($\langle \Delta r^2 \rangle \approx v_0^2 t^2$ [55], see SM [50]). Positive (blue) and negative (green) curvities ($\kappa_{\pm} \approx \pm 0.1/\text{cm} \approx \pm 0.3/b_0$) were measured following a previously described procedure [42, 49] (see Fig. 1c and SM [50]). In short, an adjustable, constant, lateral force was introduced by tilting the Perspex plate ($\vec{f} = mg \sin \varphi \hat{x}$). At a constant force, Eqs. 2, 3 reduce to a simple over-damped pendulum ($\dot{\theta} = -\kappa \mu f_0 \sin \theta$), which can be fitted by $\theta(t) = 2 \text{atan}(e^{\kappa v_0 t})$ for a perpendicular initial condition ($\hat{e}(t=0) \perp \vec{f}$).

The condition for effective attraction in Eq. 1 was then tested experimentally by dressing the robots with skirts of variable diameters: 6–24 cm ($1 \leq b/b_0 \leq 4$, see Fig. 2d

and SM [50]). We placed pairs of robots facing ($\alpha = \beta = \pi$) and touching ($r = 2b$) each other, turned them on, and monitored their center-to-center separation (r) until they no longer touch ($r > 2b$), defining the kissing time (τ_k). Figure 2e shows that when the condition for attraction is met (Eq. 1), the kissing time increases by more than two orders of magnitude. This shows experimentally that the geometric condition correctly captures the attraction between a pair of skirt-wearing-robots.

Many-body dynamics at zero orientational noise. We next show that the condition for effective attraction in Eq. 1 extends beyond zero concentration (pair-interaction), and quantitatively predicts clustering and crystallization at finite filling fractions, ϕ . The many-body generalization of Eqs. 2, 3 reads

$$\vec{v}_i = \hat{e}_i + \frac{\mu F_0}{v_0} \sum_{i \neq j} \Gamma(r_{ij}) \hat{r}_{ij} \quad (9)$$

$$\frac{d}{dt} \hat{e}_i = \kappa \sigma \hat{e}_i \times (\vec{v}_i \times \hat{e}_i) + \sqrt{2/Pe} \xi_i(t) \hat{e}_i^{\perp}, \quad (10)$$

with a range σ harmonic repulsion, $\Gamma(r_{ij}) = \min[0, k(1 - r/\sigma)]$, and a Gaussian orientational noise ($\xi_i(t)$), with a finite persistence length, $\ell_P \equiv v_0/D_r$ that defines the Péclet number $Pe = \ell_P/\sigma$. We set $\mu F_0/v_0 = 1$ and $k = 100$, leading to $2b = 0.99\sigma$ and simulate Langevin dynamics of $N = 8192$ particles (see SM [50]).

We first perform simulations at zero noise, ($1/Pe = 0$), in 1,500 different combinations of curvities ($-1 < \kappa b < 0.5$), and filling fractions ($0.001 \leq \phi \leq 0.90$) that follow Eqs. 9, 10. Each simulation runs for a total time of $10^4 \sigma/v_0$. The mean force on each particle, $\langle F \rangle$, reveals three distinct behaviors in the $\phi - \kappa b$ phase diagram (Fig. 3(a)): (i) At the top, a flocking phase where the particles have positive force alignment ($\kappa > 0$) is indicated by a vanishing average force; (ii) When curvity

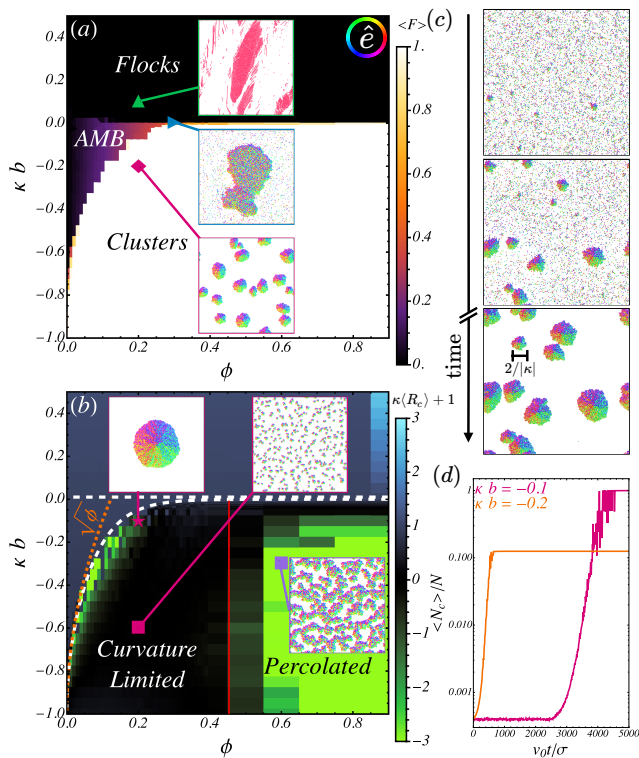


FIG. 3. **Curvity-controlled cluster size.** (a) Phase-diagram ($\phi - \kappa b$) measuring the average force on each particle, $\langle F \rangle$, without noise. Three types of steady states are identified (snapshots in insets; green upward triangle: flock; blue triangle: active fluid with MIPS; magenta diamond: clusters). In all snapshots, colors represent the orientation of \hat{e} , see color wheel top-right. (b) Intensity map of $\kappa \langle R_c \rangle + 1$. The phases identified in (a) are sketched with dashed white lines, and a $\sqrt{\phi}$ behavior at small ϕ is highlighted by an orange dashed line. A solid red line indicates the onset of percolation, at $\phi_{cp}/2$. Snapshots illustrate the difference between clusters with high curvature (magenta square) and low curvature (magenta star). (c) Cluster growth dynamics at $\kappa b = -0.2$ and $\phi = 0.2$. (d) Growth of the average number of particles in a cluster for $\kappa b = -0.1$ (red), and $\kappa b = -0.2$ (orange) with $\phi = 0.2$.

is weakly non-positive, we report an active fluid phase, with a force that grows continuously with concentration, and undergoes MIPS [36] at elevated densities, much like Active Model B (AMB) [34]; (iii) At more negative values of curvity, an arrested, clustered crystalline phase is shown by a force that exactly compensates self-propulsion (white region). The flocking and crystalline nature of the phases are confirmed by the mean polar $m = |\langle \hat{e} \rangle|$ and hexatic [56] order parameters (see SM [50]). At vanishing filling fraction ($\phi_{\min} = 10^{-3}$), the onset of clustering is well captured by the same geometric criterion (Eq. 1): $\kappa b = -1$. With increasing concentrations, particles can become effectively attracted even at less negative κb values. A cluster with an effective radius larger than the particles ($R_c > b$) becomes similarly attractive when

$$\kappa + 1/R_c < 0. \quad (11)$$

This is illustrated in Fig. 3(b) where the intensity now represents the product $\kappa \langle R_c \rangle$, with $\langle R_c \rangle$ the average clus-

ter radius (see SI): the whole clustered phase verifies $\kappa \langle R_c \rangle < -1$ (black to green intensities), with a large region that nearly saturates the inequality, so that the typical cluster size is given directly by $\langle R_c \rangle \approx -1/\kappa$. Using a simple kinetic theory in conjunction with Eq. 11, offers a clustering condition at finite concentration,

$$\kappa_c b < -1 + C\sqrt{\phi}, \quad (12)$$

and quantitatively captures the boundary between the phases (orange dashed line in Fig. 3(b), see SM [50]). This criterion means that below the clustering line, the size of clusters diminishes with increasing attraction strength (κb more negative, see insets of Fig. 3(b)). Near the clustering line, the critical cluster size may be so large that a single cluster forms. Above half close-packing, $\phi \gtrsim \phi_{cp}/2$, the system has a single percolating cluster. A cluster growth sequence (below percolation) shows the concluding typical cluster radius of $\sim 1/\kappa$ (Fig. 3(c)). We also show in Fig. 3(d) and in SM [50] videos of the time evolution of the average number of particles per cluster at two different κb 's. The growth is typical of non-critical nucleation-growth dynamics: clusters remain small over long times, until a critical size is reached, triggering a rapid (here, exponential) growth, similar to previous reports on the accumulation of very persistent self-propelled particles [57]. Steady-state mean diameter is self-limited, reaching a κ -dependent plateau.

Previous work showed flocking of self-propelled particles with positive force-alignment [58], consistent with our findings: polar order is observed at the smallest positive curvity ($\kappa b = 0.005$), and at the lowest filling fraction tested ($\phi = 0.001$), and is expected for a stiff potential (see SM [50]). By contrast, the onset of effective attraction requires a combination of finite (negative) curvity or finite concentration (Eq. 12). Otherwise, the attractive fixed point in the dynamical system (Eqs. 6-8) is unstable and the phase is indistinguishable from Active model B [34], where a low density uniform isotropic liquid undergoes MIPS at a higher density, even at zero noise [59–61].

Phase behavior at finite noise. So far we discussed deterministic dynamics with zero orientational noise ($1/Pe \rightarrow 0$ in Eq. 10). With no fluctuations, the system settles when a mechanical force balance is achieved — the clusters are arrested. In this final section, we show that the observed phases are stable even when particles have orientational diffusion.

Finite noise introduces a finite persistence length (ℓ_p), the third key parameter in our geometric condition of cohesion. The persistence length sets the characteristic curvature of an individual particle trajectory [50], which also couples to the particle's radius and curvity. Figure 4 shows that the noiseless phase diagram is qualitatively preserved, even in the presence of fluctuations ($Pe = 50$) — the same 3 distinct phases are observed even

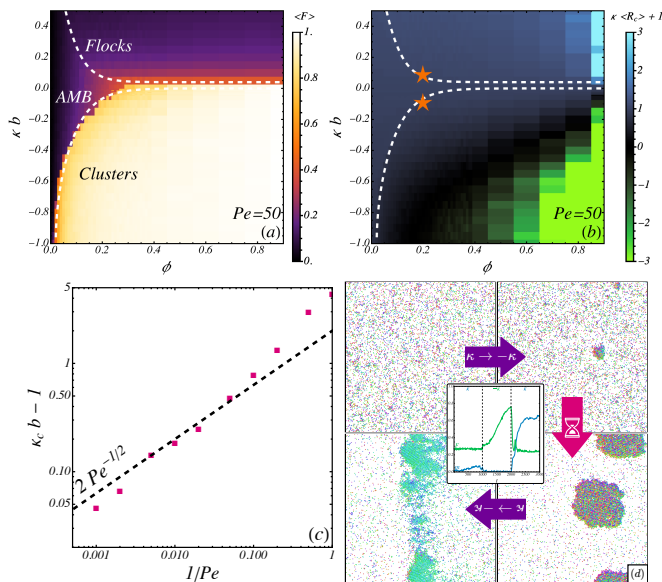


FIG. 4. **Curvity controlled cluster-size and cluster-flock transition at finite noise.** (a) Intensity map of the mean force felt by particles in the $\phi, \kappa b$ plane at $Pe = 50$ and (b) corresponding $\kappa \langle R_c \rangle$ map. Dashed white lines indicate phase boundaries. (c) Asymptotic zero-density $\kappa_c b - 1$ against $1/Pe$, in log scales. A dashed line shows $2Pe^{-1/2}$ (Eq. 13) (d) Example control strategy: switching κ to $-\kappa$ enables a user to triggers fast clustering, then long-lived flocking as $\kappa \rightarrow -\kappa$ again. Inset: example curves for magnetization m (blue) and average force F (green) with switches at dashed black lines. Parameters are shown as orange stars in (b).

though the dynamics are no longer arrested (see Videos in SM [50]). This is also captured quantitatively: while the AMB-clustering phase boundary remains sharp, the average force on each particle is too low to ensure mechanical equilibrium ($\mu \langle F \rangle / v_0 < 1$). As before, the same phase boundary is observed when measuring the polar and hexatic order parameters (see SM [50]). A similar picture is also painted for the curvity limited cluster size (Fig. 4(b)): when the curvity is not sufficiently negative to satisfy the condition for pair cohesion (Eq. 1) but the concentration is sufficiently high, the typical cluster size is again $R_c \approx -1/\kappa$ (Eq. 11). Fluctuations allow individual particles to adhere to or detach from a given cluster, yet the typical cluster size is maintained at steady-state, in a dynamical equilibrium (see Video in SM [50]). The onset of attraction at the infinite dilution limit is shifted in the presence of noise, but the shift is also quantitatively captured by extending the geometric criterion to finite persistence lengths (see SM [50]),

$$\kappa + \frac{1}{b} + \frac{2}{\sqrt{b\ell_p}} < 0. \quad (13)$$

Figure 4c shows that the $1/\sqrt{\ell_p}$ ($1/\sqrt{Pe}$) scaling above quantitatively captures the onset of attraction at infinite dilution for over 2 orders of magnitude of orientational noise ($0 < 1/Pe < 0.1$) then starts growing faster when the particles' persistence is not much larger than their

own size ($1/Pe > 0.1$).

The above results offer a microscopic handle for programmable self-assembly of self-limiting clustering, with important applications in the design of mechanical [62] and photonic [63] meta-materials, and in living matter [64]. We further show its application as a novel control architecture for a multi-agent robotic system. At non-zero noise and density, self-propelled particles do not flock even at significant curvities ($\kappa b \approx 1$). Since the curvity and the particle's radius are not mechanically independent [41, 42], inducing flocking by arbitrarily increasing κb is not always technically feasible. We propose toggling the curvity's sign as an alternative route (while roughly keeping its magnitude). This was achieved with the robots above by switching the orientation of their soft-legs (see Fig. 1(a)). A sequence of two curvity flips can lead to flocking even at globally low concentrations and finite persistence length: starting from a disordered fluid (low ϕ and $\kappa > 0$) switching to $-\kappa$, most of the particles spontaneously cluster. Due to their high local density, switching back to $\kappa > 0$, the swarm spontaneously flocks. Figure 4(d) and the corresponding video in SM [50] show that following the curvity sign-flip the exponential cluster growth expedites the flocking.

Conclusions. In this work we presented a geometric criterion for the onset of attraction and effective cohesion between pairs of robots, which depends on the coupling between two intrinsic properties of self-propelled particles: 1. their morphological curvature, $1/b$ (inverse radius), and 2. their curvity, κ : the signed, charge-like property of self-propelled particles that characterized the curving of their trajectories when subjected to an external force. The criterion (Eq. 1) shares mathematical structure with the Young-Laplace equation [65], where the stability of a three-dimensional fluid interface is conditioned by the sum of two local curvatures, suggesting a link between interfacial phenomena, boundaries, and active matter [66]. We showed that these can be designed with real robots, and found experimentally and numerically that the geometric criterion predicts the onset of effective pair attractions. The infinite dilution limit extends to finite concentrations and finite noise, and explains the typical cluster size observed, offering a powerful microscopic rule for tuning a macroscopic length scale, with important applications in material science and in living matter. Experimentally, our work focused on macroscopic robots, but force-alignment has been reported in micro-organism [67], suggesting the results above could be translated into the active field of colloidal engineering [16, 68–70]. We proposed how this construction can be used as a new control paradigm in multi-agent robotic systems, its broader applicability in dry active matter, and implication for biological and robotic swarms.

Acknowledgements. M.C. would like to thank Satyam Anand for insightful discussions on this work. E.A would like to thank Doron Markovich for design suggestions.

M.C. and S.M. acknowledge the Simons Center for Computational Physical Chemistry for financial support. This work was supported in part through the NYU IT High Performance Computing resources, services, and staff expertise. Y.L. acknowledges the support of the Israeli Science Foundation, grants 2096/18 and 2117/22. M.Y.B.Z acknowledges the support of the Dutch Brain Interface Initiative (DBI2) with project number 024.005.022 of the research programme Gravitation, which is financed by the Dutch Ministry of Education, Culture and Science (OCW) via the Dutch Research Council (NWO).

* matanzb@gmail.com

- [1] J. Toner, Y. Tu, and S. Ramaswamy, Hydrodynamics and phases of flocks, *Annals of Physics* **318**, 170 (2005).
- [2] C. Nardini, E. Fodor, E. Tjhung, F. van Wijland, J. Tailleur, and M. E. Cates, Entropy production in field theories without time reversal symmetry: Quantifying the non-equilibrium character of active matter, *Physical Review X* **7**, 021007 (2017).
- [3] S. Ro, B. Guo, A. Shih, T. V. Phan, R. H. Austin, D. Levine, P. M. Chaikin, and S. Martiniani, Model-Free Measurement of Local Entropy Production and Extractable Work in Active Matter, *Physical Review Letters* **129**, 220601 (2022).
- [4] T. Vicsek, A. Czirók, E. Ben-Jacob, I. Cohen, and O. Shochet, Novel type of phase transition in a system of self-driven particles, *Physical Review Letters* **75**, 1226 (1995).
- [5] M. Casiulis, M. Tarzia, L. F. Cugliandolo, and O. Dauchot, Velocity and speed correlations in hamiltonian flocks, *Physical Review Letters* **124**, 10.1103/PhysRevLett.124.198001 (2020).
- [6] M. Fruchart, R. Hanai, P. B. Littlewood, and V. Vitelli, Phase transitions in non-reciprocal active systems, *Nature* **592**, 363 (2021).
- [7] Q. L. Lei, M. P. Ciamarra, and R. Ni, Non-Equilibrium strongly hyperuniform fluids of circle active particles with large local density fluctuations, *Science Advances* **5**, eaau7423 (2019).
- [8] M. Casiulis, M. Tarzia, L. F. Cugliandolo, and O. Dauchot, Order by disorder: saving collective motion from topological defects in a conservative model, *Journal of Statistical Mechanics: Theory and Experiment* **2020**, 013209 (2020).
- [9] D. Levis and B. Liebchen, Simultaneous phase separation and pattern formation in chiral active mixtures, *Physical Review E* **100**, 012406 (2019).
- [10] B. Zhang and A. Snezhko, Hyperuniform Active Chiral Fluids with Tunable Internal Structure, *Physical Review Letters* **128**, 218002 (2022).
- [11] M. Casiulis and D. Levine, Emergent synchronization and flocking in purely repulsive self-navigating particles, *Physical Review E* **106**, 044611 (2022).
- [12] X.-q. Shi and F. Cheng, Extreme Spontaneous Deformations of Active Crystals, *Physical Review Letters* **131**, 108301 (2023).
- [13] B. Adorjányi, A. Libál, C. Reichhardt, and C. J. O. Reichhardt, Motility Induced Phase Separation and Frustration in Active Matter Swarms, *Physical Review E* **109**, 024607 (2024).
- [14] Y. Lei and R. Ni, Non-equilibrium dynamic hyperuniform states, *Arxiv Preprint*, 2405.12818 (2024).
- [15] D. Levis, I. Pagonabarraga, and B. Liebchen, Activity Induced Synchronization: From mutual flocking to chiral self-sorting, *Physical Review Research* **1**, 023026 (2019).
- [16] M. Y. B. Zion, Y. Caba, A. Modin, and P. M. Chaikin, Cooperation in a fluid swarm of fuel-free micro-swimmers, *Nature Communications* **13**, 184 (2022).
- [17] S. Anand, X. Ma, S. Guo, S. Martiniani, and X. Cheng, Transport and Energetics of Bacterial Rectification, *Arxiv Preprint*, 2308.08421 (2024).
- [18] Y. Tajima, K. Takimoto, and T. Nagatani, Pattern formation and jamming transition in pedestrian counter flow, *Physica A: Statistical Mechanics and its Applications* **313**, 709 (2002).
- [19] A. Cavagna and I. Giardina, Bird Flocks as Condensed Matter, *Annual Review of Condensed Matter Physics* **5**, 183 (2014).
- [20] M. Rubenstein, A. Cornejo, and R. Nagpal, Programmable self-assembly in a thousand-robot swarm, *Science* **345**, 795 (2014).
- [21] F. Alonso-Marroquín, J. Busch, C. Chiew, C. Lozano, and Á. Ramírez-Gómez, Simulation of counterflow pedestrian dynamics using spheropolygons, *Physical Review E* **90**, 063305 (2014).
- [22] A. Cavagna, I. Giardina, and T. S. Grigera, The physics of flocking: Correlation as a compass from experiments to theory, *Physics Reports* **728**, 1 (2018).
- [23] T. Sugi, H. Ito, M. Nishimura, and K. H. Nagai, *C. elegans* collectively forms dynamical networks, *Nature Communications* **10**, 683 (2019).
- [24] G. Wang, T. V. Phan, S. Li, M. Wombacher, J. Qu, Y. Peng, G. Chen, D. I. Goldman, S. A. Levin, R. H. Austin, and L. Liu, Emergent field-driven robot swarm states, *Physical Review Letters* **126**, 108002 (2021).
- [25] J. F. Boudet, J. Lintuvuori, C. Lacouture, T. Barois, A. Deblais, K. Xie, S. Cassagnere, B. Tregon, D. B. Brückner, J. C. Baret, and H. Kellay, From collections of independent, mindless robots to flexible, mobile, and directional superstructures, *Science Robotics* **6**, eabd0272 (2021).
- [26] Y. Mirhosseini, M. Y. B. Zion, O. Dauchot, and N. Bredeche, Adaptive phototaxis of a swarm of mobile robots using positive and negative feedback self-alignment, in *Proceedings of the Genetic and Evolutionary Computation Conference (ACM, 2022)* pp. 104–112.
- [27] J. D. Weeks, D. Chandler, and H. C. Andersen, Role of repulsive forces in determining the equilibrium structure of simple liquids, *The Journal of Chemical Physics* **54**, 5237 (1971).
- [28] J.-P. Hansen and I. R. McDonald, *Theory of simple liquids* (Elsevier Academic Press, 2006).
- [29] M. Kardar, *Statistical Physics of Particles* (Cambridge University Press, 2007).
- [30] L. Onsager, Statistical hydrodynamics, *Il Nuovo Cimento Series 9* **6**, 279 (1949).
- [31] N. Oppenheimer, D. B. Stein, M. Y. B. Zion, and M. J. Shelley, Hyperuniformity and phase enrichment in vortex and rotor assemblies, *Nature Communications* **13**, 804 (2022).
- [32] Y. Shoham and N. Oppenheimer, Hamiltonian dynamics

- and structural states of two-dimensional microswimmers, *Physical Review Letters* **131**, 178301 (2023).
- [33] M. C. Marchetti, J. F. Joanny, S. Ramaswamy, T. B. Liverpool, J. Prost, M. Rao, and R. A. Simha, Hydrodynamics of soft active matter, *Reviews of Modern Physics* **85**, 1143(47) (2013).
- [34] M. E. Cates and J. Tailleur, Motility-Induced Phase Separation, *Annual Review of Condensed Matter Physics* **6**, 219 (2014).
- [35] A. P. Solon, J. Stenhammar, M. E. Cates, Y. Kafri, and J. Tailleur, Generalized thermodynamics of motility-induced phase separation: Phase equilibria, laplace pressure, and change of ensembles, *New Journal of Physics* **20**, 10.1088/1367-2630/aacdd (2018).
- [36] J. Tailleur and M. E. Cates, Statistical mechanics of interacting run-and-tumble bacteria, *Physical Review Letters* **100**, 218103 (2008).
- [37] J. Zhang, R. Alert, J. Yan, N. S. Wingreen, and S. Granick, Active phase separation by turning towards regions of higher density, *Nature Physics* **17**, 961 (2021).
- [38] R. G. Winkler, A. Wysocki, and G. Gompper, Virial pressure in systems of spherical active Brownian particles, *Soft Matter* **11**, 6680 (2015).
- [39] L. Caprini, U. Marini Bettolo Marconi, and A. Puglisi, Spontaneous Velocity Alignment in Motility-Induced Phase Separation, *Physical Review Letters* **124**, 78001 (2020).
- [40] L. Caprini, C. Maggi, and U. M. B. Marconi, Collective effects in confined Active Brownian Particles, *Journal of Chemical Physics* **154**, 244901 (2021).
- [41] P. Baconnier, O. Dauchot, V. Démery, G. Düring, S. Henkes, C. Huepe, and A. Shee, Self-Aligning Polar Active Matter, *Arxiv Preprint* , 1 (2024), arXiv:2403.10151.
- [42] E. Arbel, N. Oppenheimer, Y. Lahini, and M. Y. B. Zion, A mechanical origin of cooperative transport, *Arxiv cond-mat.soft* , 1 (2024).
- [43] O. Dauchot and V. Démery, Dynamics of a self-propelled particle in a harmonic trap, *Physical Review Letters* **122**, 1 (2019).
- [44] C. A. Weber, T. Hanke, J. Deseigne, S. Léonard, O. Dauchot, E. Frey, and H. Chaté, Long-Range Ordering of Vibrated Polar Disks, *Physical Review Letters* **110**, 208001 (2013).
- [45] K.-D. Nguyen Thu Lam, M. Schindler, and O. Dauchot, Self-propelled hard disks: Implicit alignment and transition to collective motion, *New Journal of Physics* **17**, 113056 (2015).
- [46] K.-D. N. T. Lam, M. Schindler, O. Dauchot, K.-D. Nguyen, T. Lam, M. Schindler, and O. Dauchot, Polar active liquids: a universal classification rooted in nonconservation of momentum, *Journal of Statistical Mechanics: Theory and Experiment* **2015**, P10017 (2015).
- [47] H. Chaté, Dry Aligning Dilute Active Matter, *Annual Review of Condensed Matter Physics* **11**, 189 (2020).
- [48] J. D. Jackson, *Classical Electrodynamics* (Wiley, 1999).
- [49] M. Y. B. Zion, J. Fersula, N. Bredeche, and O. Dauchot, Morphological computation and decentralized learning in a swarm of sterically interacting robots, *Science Robotics* **8**, 1 (2023).
- [50] URL_will_be_inserted_by_publisher.
- [51] A. P. Thompson, H. M. Aktulga, R. Berger, D. S. Bolinteanu, W. M. Brown, P. S. Crozier, P. J. in 't Veld, A. Kohlmeyer, S. G. Moore, T. D. Nguyen, R. Shan, M. J. Stevens, J. Tranchida, C. Trott, and S. J. Plimpton, LAMMPS - a flexible simulation tool for particle-based materials modeling at the atomic, meso, and continuum scales, *Computer Physics Communications* **271**, 10.1016/j.cpc.2021.108171 (2022).
- [52] S. H. Strogatz, *Nonlinear Dynamics and Chaos* (CRC Press, 2018) p. 501.
- [53] D. B. Allan, T. Caswell, N. C. Keim, and C. M. van der Wel, Trackpy: Fast, flexible particle-tracking toolkit (2014).
- [54] T. Walter and I. D. Couzin, Trex, a fast multi-animal tracking system with markerless identification, and 2d estimation of posture and visual fields, *eLife* **10**, 1 (2021).
- [55] J. R. Howse, R. A. L. Jones, A. J. Ryan, T. Gough, R. Vafabakhsh, and R. Golestanian, Self-motile colloidal particles: From directed propulsion to random walk, *Physical Review Letters* **99**, 048102 (2007).
- [56] D. R. Nelson and B. I. Halperin, Dislocation-mediated melting in two dimensions, *Physical Review B* **19**, 2457 (1979).
- [57] P. Cremer and H. Löwen, Scaling of cluster growth for coagulating active particles, *Physical Review E - Statistical, Nonlinear, and Soft Matter Physics* **89**, 022307 (2014).
- [58] J. Deseigne, O. Dauchot, and H. Chaté, Collective motion of vibrated polar disks, *Physical Review Letters* **105**, 098001 (2010).
- [59] A. P. Solon, Y. Fily, A. Baskaran, M. E. Cates, Y. Kafri, M. Kardar, and J. Tailleur, Pressure is not a state function for generic active fluids, *Nature Physics* **11**, 673 (2015).
- [60] P. Nie, J. Chatteraj, A. Piscitelli, P. Doyle, R. Ni, and M. Pica Ciamarra, Stability phase diagram of active Brownian particles, *Physical Review Research* **2**, 023010 (2020).
- [61] M. Casilius, D. Hexner, and D. Levine, Self-propulsion and self-navigation: Activity is a precursor to jamming, *Physical Review E* **104**, 064614 (2021).
- [62] K. Bertoldi, V. Vitelli, J. Christensen, and M. V. Hecke, Flexible mechanical metamaterials (2017).
- [63] J. D. Joannopoulos, S. G. Johnson, J. N. Winn, and R. D. Meade, *Photonic Crystals Molding the Flow of Light*, 2nd ed. (Princeton University Press, 2008) p. 305.
- [64] M. F. Hagan and G. M. Grason, Equilibrium mechanisms of self-limiting assembly, *Reviews of Modern Physics* **93**, 10.1103/RevModPhys.93.025008 (2021).
- [65] P.-G. de Gennes, F. Brochard-Wyart, and D. Quere, *Capillarity and Wetting Phenomena* (Springer, 2002) p. 291.
- [66] F. Turci, R. L. Jack, and N. B. Wilding, Partial and complete wetting of droplets of active brownian particles, *Soft Matter* **20**, 2060 (2024).
- [67] A. M. Roberts, The mechanics of gravitaxis in paramecium, *Journal of Experimental Biology* **213**, 4158 (2010).
- [68] M. Y. B. Zion, Y. Caba, R. Sha, N. C. Seeman, and P. M. Chaikin, Mix and match - a versatile equilibrium approach for hybrid colloidal synthesis, *Soft Matter* **16**, 4358 (2020).
- [69] T. Hueckel, G. M. Hocky, and S. Sacanna, Total synthesis of colloidal matter, *Nature Reviews Materials* **6**, 1053 (2021).
- [70] A. Modin, M. Y. B. Zion, and P. M. Chaikin, Hydrodynamic spin-orbit coupling in asynchronous optically driven micro-rotors, *Nature Communications* **14**, 4114 (2023).